Supplementary Materials:

K2P channel gating mechanisms revealed by structures of TREK-2 and a complex with Prozac

Authors: Yin Yao Dong[†], Ashley C.W. Pike[†], Alexandra Mackenzie, Conor McClenaghan, Prafulla Aryal, Liang Dong, Andrew Quigley, Mariana Grieben, Solenne Goubin, Shubhashish Mukhopadhyay, Gian Filippo Ruda, Michael V. Clausen, Lishuang Cao, Paul E. Brennan, Nicola A. Burgess-Brown, Mark S. P. Sansom, Stephen J. Tucker[2]*, Elisabeth P. Carpenter*.

* Correspondence to: liz.carpenter@sgc.ox.ac.uk and stephen.tucker@physics.ox.ac.uk.

This PDF file includes:

Materials and methods

Figs. S1 to S10

Tables S1

Reference List

Materials and Methods:

Cloning and expression

The gene for TREK-2 (KCNK10) was purchased from the Mammalian Gene Collection (MGC:104160, IMAGE: 30915621, BC075021). The construct used for structure determination consisted of residues Gly^{67} to Glu^{340} of TREK-2, with a C-terminal purification tag with a tobacco etch virus (TEV) protease cleavage site, a 10x His purification sequence and a FLAG tag, in the expression vector pFB-CT10HF-LIC (available from the SGC). Baculoviruses were produced by transformation of DH10Bac cells. *Spodoptera frugiperda* (Sf9) insect cells in Sf-900 II SFM medium (Life Technologies) were infected with recombinant baculovirus and incubated for 65 h at 27 °C in shaker flasks.

Purification of TREK-2

Cell pellets from 1 litre of insect cell culture were resuspended in 50 ml of extraction buffer (50 mM HEPES, pH 7.5, 200 mM KCl, 5 mM imidazole, Roche protease inhibitor cocktail) and lysed by two passes through an EmulsiFlex-C5 homogenizer (Aventis). Protein was extracted from cell membranes by incubation of the crude lysate with 1 % (w/v) OGNG and 0.1 % (w/v) CHS for 1 h at 4 ℃. Cell debris and unlysed cells were removed by centrifugation at 35,000 g for 1 h. Detergent-solubilized protein was purified by immobilized metal affinity chromatography by batch binding to Co^{2+} charged TALON resin (Clontech) at 4 ℃ for 1 h. The resin was washed with 30 column volumes of wash buffer (50 mM HEPES, pH 7.5, 200 mM KCl, 20 mM imidazole, 0.18 % OGNG and 0.018 % CHS) and eluted with wash buffer supplemented with 250 mM imidazole. The eluted protein was desalted using a PD10 column (GE healthcare) pre-equilibrated with extraction buffer containing 0.18 % OGNG and 0.018 % CHS. Desalted protein was subsequently treated with 10:1 TEV protease and 20:1 PNGaseF (w:w, protein:enzyme) overnight at 4 ℃. The TEV and PNGaseF treated protein was separated from the 6x His-tagged enzymes and uncleaved TREK-2 by incubation for 1h with TALON resin at 4 °C. The resin was collected in a column and the flow-through and initial wash with extraction buffer were collected and concentrated to 0.5 ml using a 30 kDa cut-off concentrator (Corning). The concentrated protein was further purified by size exclusion chromatography (SEC) using a Superose 6 10/300GL column (GE Healthcare) equilibrated with SEC buffer (20 mM HEPES, pH 7.5, 200 mM KCl, 0.12 % OGNG and 0.012 % CHS) (fig. S1). The four peak fractions (0.5 ml fractions) containing the highest

protein concentration were combined and concentrated in a 2 ml 30 kDa concentrator (Sartorius) for crystallization (fig. S1B).

Crystallization of TREK-2

Protein was concentrated to 20 mg/ml, then diluted to 9–12 mg/ml using SEC buffer without added detergent. Initial crystals were grown at 4ºC from sitting drops (150-200 nl) set up in 96-well format using a Mosquito crystallization robot (TTP Labtech) and protein:reservoir ratios of 2:1, 1:1 and 1:2. Two crystal forms of TREK-2 were observed depending on the crystallization conditions. Form 1 (up state) crystals were initially obtained in an in-house version of MemGold HT-96 screen (Molecular Dimensions) (*39*) condition H11. Form 1 crystallization conditions were optimized to give a final reservoir solution containing 31 % (v/v) polyethylene glycol (PEG) 400, 1 mM cadmium chloride, 2 % (w/v) benzamidine, 0.1 M HEPES, pH 8.0. Form 2 (down state) crystals were obtained in MemGold2 (Molecular Dimensions) (*40*) conditions E4 and G11. Optimized crystals were grown from 150 nl drops comprising 90 nl protein solution (12.1 mg/ml) and 60 nl reservoir solution containing 22 % (w/v) PEG1500, 3 % (v/v) methanol, 0.1 M sodium cacodylate, pH 6.5.

Form 1 crystals were cryo-cooled by slow transfer into artificial mother liquor containing 0.2 M potassium chloride, 2 % (w/v) benzamidine, 0.2 % OGNG / 0.02 % CHS, 0.1 M HEPES pH8.0, 35 % (v/v) PEG400 followed by plunging into liquid nitrogen. Form 2 crystals were similarly equilibrated against solutions containing increasing concentrations of PEG1500 (22-35 %) prior to cryo-cooling in liquid nitrogen. Diffraction of the form 1 crystals was improved by slowly increasing the concentration of PEG400 to above 35 % (v/v) which resulted in a 10 % shrinkage in unit cell volume compared to untreated crystals.

Racemic Br-fluoxetine synthesis:

Racemic 3-(2-bromo-4-(trifluoromethyl)phenoxy)-*N*-methyl-3-phenylpropan-1-amine **3** was prepared following the reported procedure for the synthesis of fluoxetine (*41*), starting from 2-bromo-1-fluoro-4-(trifluoromethyl)benzene **2** and 3-methylamino-1-phenylpropanol **1** (fig. S10). The title compound was converted into its hydrochloride salt by addition of a dry HCl in diethyl ether to a solution of **1** in dry diethyl ether.

LCMS [ES$^+$]: Rt 7.0; m/z (rel. abundance): 388.02 (95), 389.03 (20), 390.02 (100), 391,02 (25) [M+H]$^+$.

^{1}H NMR (400 MHz, DMSO-d_6) δ 7.93 (1H, d, J=1.7 Hz), 7.58 (1H, dd, J=1.8, 8.7 Hz), 7.40 - 7.37 (4H, m), 7.31 - 7.26 (1H, m), 7.12 (1H, d, J=8.7 Hz), 5.70 (1H, dd, J=5.1, 7.9 Hz), 2.62 - 2.49 (2H, m), 2.27 (3H, s), 2.18 - 2.08 (1H, m), 2.01 - 1.91 (1H, m).

^{13}C NMR (101 MHz, DMSO-d_6) δ 157.3, 140.9, 130.4, 129.2, 128.3, 126.6, 126.3, 125.3, 122.9, 122.6, 122.5, 115.6, 112.5, 79.0, 47.9, 38.1, 36.5.

^{19}F NMR (376 MHz, DMSO-d_6) δ-60.08.

Crystallization of TREK-2 in complex with fluoxetine derivatives

A 50 mM stock of Br-fluoxetine or norfluoxetine (Sigma-Aldrich) was dissolved in SEC buffer without detergent. This was added to the protein to give a final compound concentration of 5 mM and protein concentration of 9-11 mg/ml. Protein was incubated with compound for 3 h at 4 ℃ prior to crystallization. Crystals were grown as for form 1 and 2 crystals with protein::reservoir ratios of 2:1 and 1:1. The norfluoxetine co-crystals grew from a reservoir solution containing 0.2 M ammonium formate, 0.1 M Tris, pH 7.0 and 30 % (w/v) pentaerythritol ethoxylate (15/4). Crystals were cryo-cooled directly from reservoir solution with added detergent (0.2 % OGNG / 0.02 % CHS). For the Br-fluoxetine derivative, reservoir solution contained 0.1 M MES buffer, pH 6.5, 0.05 M magnesium chloride, 1mM CdCl$_2$ and 14-30 % PEG500DME. Both plate ($P2_12_12_1$) and prism ($P2_1$) morphologies were observed in identical drops, however the plate morphology diffracted to higher resolution. Crystals were cryo-cooled by stepwise transfer into artificial mother liquor containing increasing concentrations of PEG500DME (0.2 M potassium chloride, 0.2 % OGNG/0.02% CHS, 0.1 M MES, pH 6.5, 1 mM CdCl$_2$, 14-30% PEG500DME). The PEG500DME concentration was increased in 5 % steps up to 30 %. 5 mM Br-fluoxetine was added to the cryo-solution in the final 30 % PEG500DME soak solution. Crystals were rapidly cryo-cooled in liquid nitrogen.

Structure determination and refinement for the form 1 crystals

All crystallographic data were collected at 100 K on either I02 (norfluoxetine complex) or the I24 microfocus beamline (Diamond Light Source) with a fine phi slicing strategy and processed with XDS (*42*) and AIMLESS (*43*). Form 1 crystals diffracted

anisotropically with diffraction spots to 3.2 Å in the best direction and 4.1 Å in the worst direction (nominal resolution 3.4 Å; limits based on Mn (I/σI) >2 criteria - see Table S1). The crystals belong to space group $P2_1$ and contain two channel homodimers per asymmetric unit. Initial phases were obtained using molecular replacement with a search model ensemble comprising the transmembrane regions of TRAAK/K2P4.1 (3UM7) and TWIK-1/K2P.1 (3UKM) monomers in PHASER ([44]). Initial maps, calculated from the poly-alanine truncated PHASER solution, clearly revealed electron density for the extracellular cap domain region and allowed placement of both cap helices (EC1/EC2) for each chain. Subsequent rounds of refinement and model building, carried out with COOT ([45]), allowed connection of the cap helices and placement of the majority of sidechains. The chain trace was verified by treatment of crystals with 1 mM sodium ethylmercurithiosalicylic acid (EMTS) overnight which gave clear labeling at a single solvent-exposed cysteine (Cys[249]) in M3 (see fig. S2D). Both prime-and-switch maps (PHENIX ([46])) and interactive B-factor sharpening in (COOT ([45])) were indispensable in the model building process. Two strong peaks that were present in both the 2mFo-DFc / mFo-DFc and anomalous difference electron density maps were assigned to cadmium ions that mediate lattice contacts between the cap domains of two adjacent homodimers in the crystal (fig S2D). The connection of the two cap helices and the intermolecular disulfide bridge between Cys[123] of each monomer could also be clearly resolved and results in a domain-exchanged topology for the TREK-2 homodimer (fig. S3). Elongated tubes of persistent electron density, bound between M3 and M4, were modeled as the alkyl chains of a single phospholipid moiety. While there are indications of lipid density on both homodimers, alkyl chains have only been modeled for the AB homodimer.

Refinement was carried out with BUSTER (v. 2.11.2) ([47]) using all data to 3.2 Å with NCS restraints and a single TLS group per protein chain. The structure was refined to R/R_{free} values of 23.7 / 25.4 %, with good model geometry (Table S1). The final model comprises two channel homodimers per asymmetric unit, encompassing residues Lys[73]-Lys[333], each containing four potassium ions within the selectivity filter. The putative glycosylated region around Ser[150] in the extracellular cap domain is completely disordered in all molecules, the M2-M3 connecting region (residues 229-235) is not ordered in chains A and C, and the filter2-M4 connecting loop (residues 293-298) is only fully ordered in the AB homodimer. The model has excellent geometry as assessed by the MOLPROBITY server ([48]) with 97.5 % of residues located in favored regions of the Ramachandran plot and no outliers.

Determination of Cap connectivity for the form 1 crystals

The electron density maps calculated for the cap region of the Form 1 crystals is sufficiently well resolved to unambiguously trace the main chain and confirm the domain-exchanged arrangement previously observed for the TRAAK-Fab structure (Fig. S4). Clear interpretation is aided by the fact that in the form 1 crystals the cap domain is stabilized in the crystal lattice by a sizeable intermolecular contact between the C-terminal ends of the EC1 helices (from chains B and D on adjacent homodimers) that is mediated by two cadmium ions from the crystallization solution. The geometry of the connecting disulfide bridge falls within the standard left-handed spiral classification based on the chi2, chi3, chi2' angles (*49*).

Structure determination and refinement for the form 2 crystals

The coordinates of a channel homodimer from the 3.4 Å Form 1 crystal form were used as a molecular replacement search model in PHASER (*44*). Form 2 crystals also contain two channel homodimers in the asymmetric unit although one dimer is considerably less ordered and has much higher overall temperature factors (Table S1). Initial electron density maps indicated a large shift in the position of M4 in the Form 2 structure and so the search model was truncated at Gly312 and the sidechains were removed prior to calculation of a prime-and-switch map in PHENIX (*46*). The positions of M2, M3 and M4 were adjusted in the better resolved dimer and sidechain positions were built *de novo*. The resultant dimer was then used as a template to build the less ordered dimer. Refinement was carried out with BUSTER (v. 2.11.2) (*47*) using all data to 3.8 Å with NCS restraints and a single TLS group per protein chain. In addition, individual temperature factors were refined as this was found to improve R_{free}. Electron density within the selectivity filter was modeled by three potassium ions. No density was observed for the most extracellular K^+ ion position in the filter. B factor sharpening in COOT (*45*) was used to improve the quality of the electron density maps so that sidechains could be assigned. Elongated tubes of electron density were observed between M3 and M4 and penetrating through the side fenestrations into intracellular pore vestibule. This density has been assigned to partial lipid alkyl chains. The final model has been refined to acceptable R/R_{free} values and geometry (Table S1).

Norfluoxetine and Br-fluoxetine structure determination

The coordinates of a channel homodimer from the Form 2 crystal form were used as a molecular replacement search model in PHASER (*44*). The models were rebuilt in COOT

(*45*) and refined with BUSTER (v. 2.11.2) (*47*) as described for Form 2. Using data collected from co-crystals of the Br-fluoxetine derivative at a wavelength close to the bromine K edge (λ=0.886Å) we unambiguously resolved the positions of the bromine atoms using anomalous difference electron density maps. Anomalous peaks were evident in all but one of the fenestrations (Fig S7A) indicating bound ligand (each channel homodimer contains two lateral fenestrations). Additional anomalous peaks were observed between the cap domains of adjacent dimers which correspond to the two cadmium ions that mediate lattice contacts. Guided by the anomalous peaks, the tri-fluoro-methylated phenoxyl group of the Br-fluoxetine ligand was unambiguously modelled into all 4 fenestrations (the Br-fluoxetine crystals contain two channel homodimers in the asymmetric unit). The remainder of the ligand appears to be disordered with little or no electron density even in sharpened maps and has not been modelled. The bromine atoms were manually assigned an occupancy of 0.8 to account for signs of radiation damage.

The norfluoxetine complex was crystallized in the same spacegroup as the Form 2 down state. Initial electron density maps showed evidence of ligand binding in a similar position within the fenestration to that observed in the Br-fluoxetine derivative. The density was relatively weak in the initial BUSTER maps (Fig. S7H), but could clearly be resolved using both B-factor sharpening in COOT, and REFMAC and RESOLVE density-averaged maps (Fig. S7 E-G). Initially, norfluoxetine was modelled into the density in the best resolved site between M4 of chain A and M2 of chain B. As the norfluoxetine used for co-crystallization was a racemic mixture, both R- and S- forms were modelled with equal occupancy. Multiple binding modes were initially explored but a single orientation similar to that observed for the Br-fluoxetine gave the best fit based on both density-fit and refinement behavior. This binding mode was then used to account for the weaker electron density in the three other fenestration sites. Ligand coordinates and restraint files were generated using the GRADE web server (http://grade.globalphasing.org). Molecular graphics were generated using either PyMol (*50*) or the UCSF Chimera package (Fig 2CD) (*51*).

Molecular dynamics simulations

Models of the TREK-2 up and down states were created using the crystallographic structures with missing atoms and loops were added back in most favored position without clashes using COOT (*45*). The up state was modeled by taking chain A and chain B of

4BW5. The missing M2-M3 loop (226-231) of chain A was modeled based on chain B, with the cap-M2 connection, residues 149 to 152 modeled based on residual electron density present for chain C. The TREK-2 down state chain A cap-M2 loop (residues 150-154), M2-M3 loop (residues 226-230) whereas chain B cap-M2 loop (residues 149-154), TM2-TM3 loop (residues 226-231), and pre-M4 loop (residues 292-297) were modeled in MD simulations using Modeller 9v9 (*52*). The resulting models were converted to coarse-grained (CG) (Martini v2.1) representations and CG-MD simulations then performed for 500 ns at 323 K to permit the assembly and equilibration of a bilayer containing POPC (1-palmitoyl-2-oleoyl-sn-glycero-3-phosphocholine) lipids around the embedded membrane protein. The POPC head groups were altered to POPC:POPE (80:20) in the extracellular leaflet and POPC:POPE:POPS (40:20:20) in the intracellular leaflet and additional coarse grain simulation was conducted for a total of 1 μs. The protein and lipids were next converted to atomistic structures using the CG2AT method described previously (*53*). The initial system was solvated with SPC water and 150 mM KCl, and three K^+ ions at position S0, S2 and S4 in the selectivity filter, whereas two water molecules were also added to the filter at the S1 and S3 positions. Atomistic simulations employed the GROMOS 53A6 united-atom force-field with SPC water (*53, 54*). The atomistic system was equilibrated for 2 ns with the non-hydrogen atoms of the protein restrained at constant pressure (1 atm) and temperature (310 K) before the 100ns unrestrained MD simulation with a timestep of 2 fs and a second 100ns simulation was repeated by randomizing initial velocity of the system. The interactions of lipids with the surface of the embedded membrane protein were evaluated with 100 ns MD simulations in which the protein conformation was restrained (via positional restraints to the C-α atoms (force constant 1000 KJ/mol/Å)). Normalized lipid densities were calculated for these simulations from the density of carbon atoms of the POP* lipids using the Volmap plugin tool with a 1 Å grid spacing.

Electrophysiology

Full length human TREK-2 (NP_612191) and the ORF encoding the truncated crystal construct were each cloned into the pBF oocyte expression vector which adds the 5' and 3' UTR sequences of the *Xenopus* β-globin gene. Mutagenesis was performed on full length TREK-2 and all mutations verified by automated sequencing. Capped mRNAs were then prepared by in vitro transcription using the AmpliCap SP6 High Yield Message Maker Kit (CamBio). Oocytes were prepared by collagenase digestion and manual defolliculation, and

rinsed in ND96 solution prior to injection with the mRNA of interest; ND96 solution contained (in mM): 96 NaCl, 2 KCl, 1.8 $CaCl_2$, 1 $MgCl_2$, 10 HEPES (pH 7.4). Cells were typically injected with 0.1-2 ng of mRNA and currents were recorded 12-24 h following injection. Giant-patch electrodes were pulled from thick-walled borosilicate glass (Harvard Apparatus) and polished to give pipette resistances around 0.5-1 MΩ when filled with pipette solution. Pipette solution contained (in mM) 116 NaCl, 4 KCl, 1 $MgCl_2$, 1.8 $CaCl_2$, 10 HEPES (pH 7.4); whilst bath solution contained (in mM) 120 KCl, 1 NaCl, 2 EGTA, 10 HEPES (pH 7.3). For measurement of intracellular pH-sensitivity the bath solution was adjusted to the indicated pH. Patches were perfused with solution via a gravity flow perfusion system. Arachidonic acid (Sigma) was dissolved in DMSO and freshly diluted to the working concentration each day. Data were acquired with pClamp v10 (Molecular Devices), currents were recorded using an Axopatch 200B (Molecular Devices), filtered at 1 kHz and sampled at 10 kHz (Digidata 1322A, Molecular Devices). Macroscopic currents from inside out patches were recorded from 250 ms voltage steps to o mV from a holding potential of -80 mV unless otherwise indicated. Data are presented as the mean ± S.E.Mvoltage ramps as described for each experiment. For tests of mechanosensitivity -11mmHg of a negative pressure of -11 mmHg was manually applied through the patch pipette and calibrated using a Druic DPI260 pressure indicator. For measurement of whole cell currents using two electrode voltage clamp: Electrodes were pulled from thick-walled borosilicate glass and filled with 3 M KCl. ND96 bath solution was used for all recordings; pH was adjusted using either NaOH or HCl. Oocytes were perfused with bath solution via a peristaltic pump perfusion system. Data were acquired with pClamp v10; currents were recorded using a GeneClamp 500 amplifier (Molecular Devices) and digitized using a Digidata 1322A.Current-voltage recordings were made by stepping membrane voltage from -120 mV to +60 mV in 10 mV increments for 300 ms from a holding potential of -80 mV. For measurement of extracellular pH sensitivity the membrane potential was ramped from -150 mV to +50 mV from a holding potential of -100 mV. Experiments were performed at room temperature (18-22 °C). All traces were analyzed using Clampfit and are presented as mean ± SEM. Planar lipid bilayer experiments were performed using a Port-a-Patch automated planar patch clamp system (Nanion Technologies GmbH). The internal buffer was 200 mM KCl, and 10 mM HEPES pH 6.0, the outside buffers was 200 mM KCl, 10 mM HEPES pH 6.0. Giant unilamellar vesicles (GUVs) of DPhPC with 10% cholesterol were made by electroformation in an ITO coated glass chamber using the Vesicle Prep Pro (Nanion Technologies GmbH). Channels were incorporated by incubating the GUVs with purified TREK-2 for an hour after which

detergents were removed by incubation with bio-beads SM-2 (Bio-Rad Laboratories)Channels were incorporated by incubating the GUVs with TREK-2 containing proteoliposomes of POPE, POPG and POPC (1:1:2 ratio). The Port-a-Patch was connected to an Axon Axopatch 200B amplifier; data were filtered at 5 kHz and recorded with a 100 kHz sampling rate.
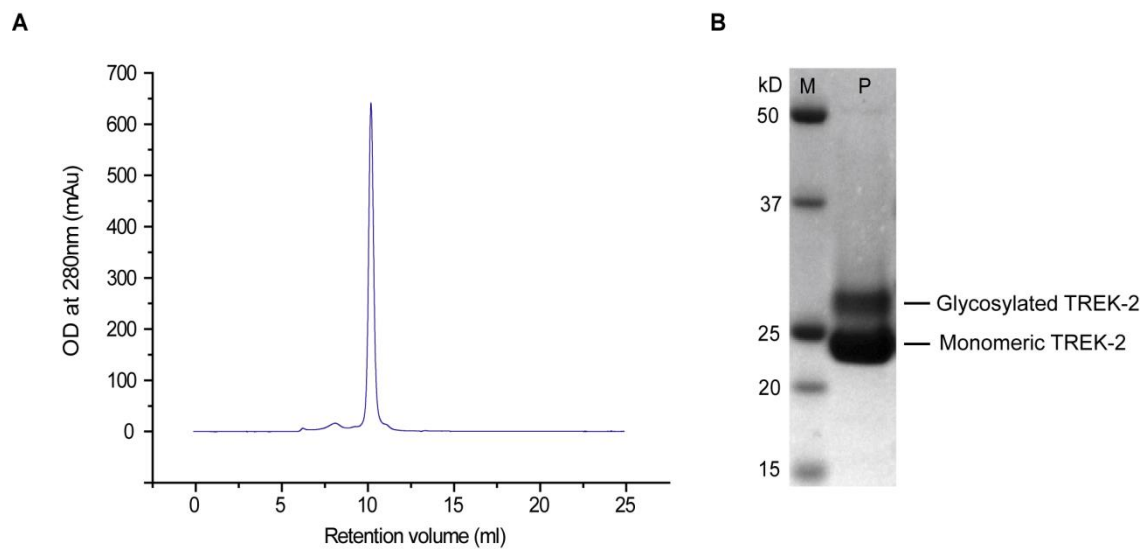
Supplementary Figures:

A

B

Fig. S1. Purification of TREK-2. (**A**) Size exclusion chromatography (SEC) profile for TREK-2 and (**B**) SDS-PAGE analysis of final pooled material (P) showing that the protein used in crystallization is partially deglycosylated by PNGaseF. M indicates protein molecular weight markers.
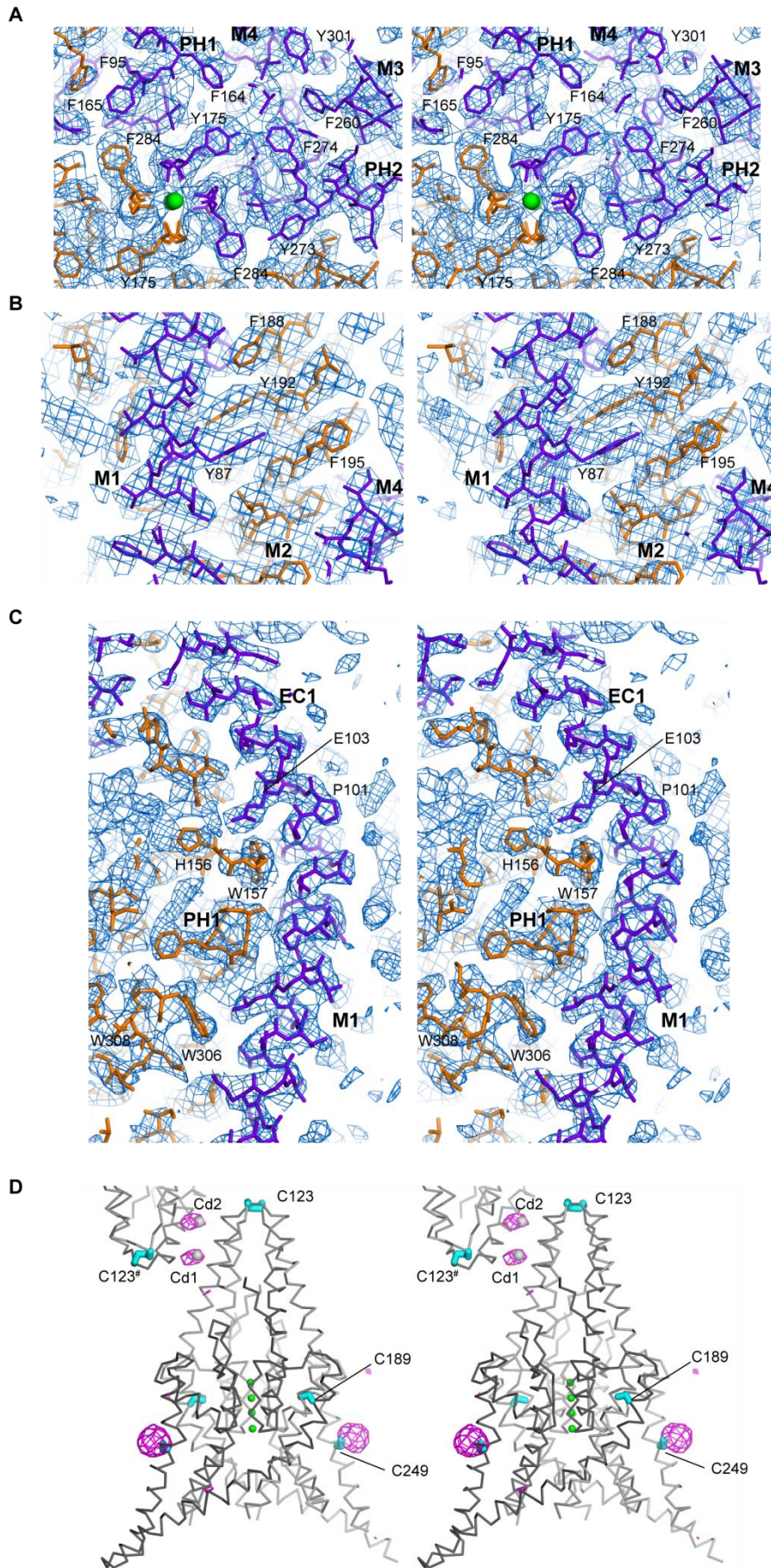
Fig. S2.

Fig. S2. **Quality of electron density for the up state 3.4 Å TREK-2 crystal structure.** (**A-C**) Representative views of electron density around the pore (**A**), M1-M2 interface (**B**) and M1-EC1 helices (**C**). The electron density map shown is a simulated-annealing, composite omit map calculated in PHENIX, contoured at 1.2σ (**A,B**; for clarity) or 1σ (**C**) and overlaid on the final model. (**D**) 6 Å anomalous difference map calculated from data collected from a crystal soaked with 1 mM EMTS. The electron density (magenta) is contoured at 3.5 σ. The solvent-exposed Cys^{249} located in M3 of each monomer is clearly identified by strong anomalous peaks (>10σ). The other two cysteines (cyan) present in TREK-2 are not labelled under these conditions – Cys^{123} forms an intermolecular disulphide bridge with its counterpart in the homodimer and Cys^{189} (M2) is completely buried. Two cadmium ions (Cd1/Cd2) from the crystallization solution, mediating lattice contacts between the cap domain EC1 helices of adjacent homodimers, are also identified in the anomalous difference map by weaker (ca. 5σ) peaks.
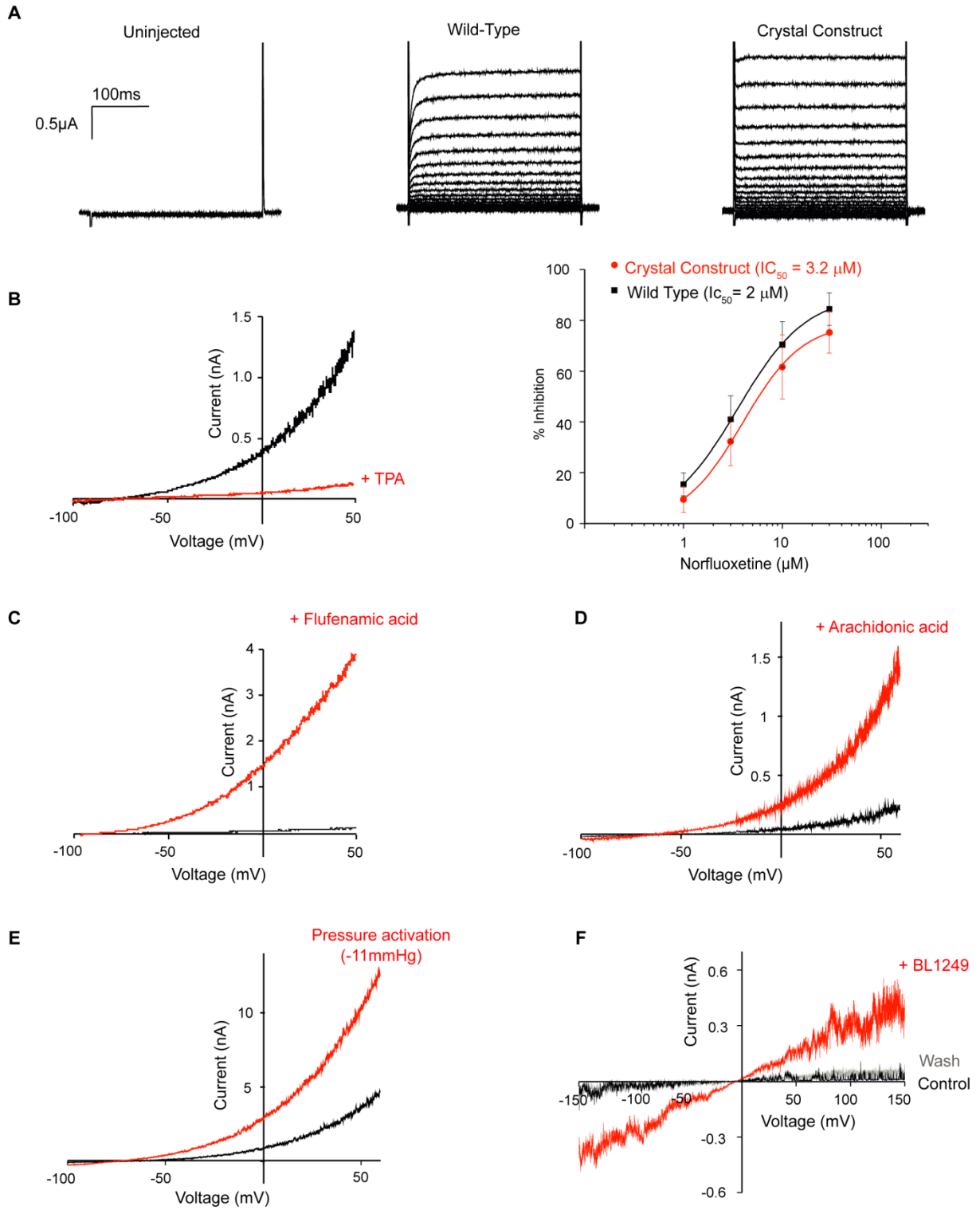
Fig. S3

Fig. S3. Wild type and crystal construct length TREK-2 show similar behavior with a range of stimuli. (**A**) Current-voltage relationship from two electrode voltage clamp recordings of the WT and truncated crystal construct channels expressed in *Xenopus* oocytes. The membrane voltage was stepped from -120 mV to +60 mV in 10 mV increments for 300 ms from a holding potential of -80 mV. (**B**) A representative trace showing block of the crystal construct channel by 1 mM Tetrapentylammonium (TPA). The channels also retain inhibition by norfluoxetine. (**C**) Flufenamic acid (FFA, 1 mM) (*55*) and (**D**) Arachidonic acid (10 μM) both activate the crystal construct channels in inside out patches. (**E**) Importantly, the truncated crystal construct also retains mechanosensitivity (-11 mm Hg). (**F**) Functional activity is also observed when the purified crystal construct protein is reconstituted into a lipid bilayer. K$^+$ selective currents from the purified protein (black trace) can be activated by 30 μM BL1249, a TREK channel activator (*55*) (red trace). This effect is reversible (wash, grey trace). Currents were recorded using a 10 s ramp from -150 mV to +150 mV.
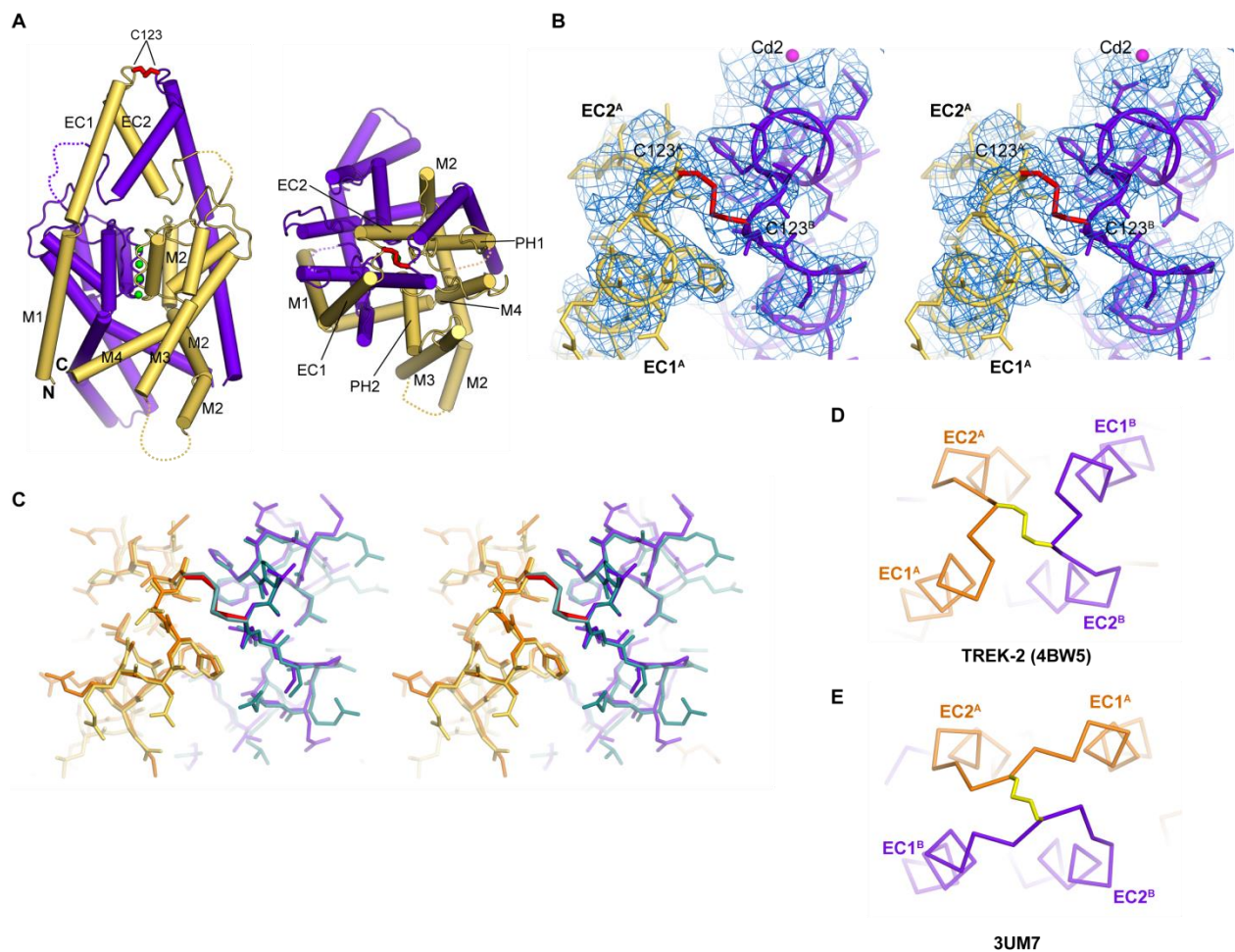
Fig. S4. The structure on TREK-2 in the vicinity of the disulfide bond at the distal end of the cap, is shown with electron density omit maps. The maps reveal a M1/EC1/EC2 domain-exchanged conformation similar to that seen in the 2.75Å TRAAK structure in complex with an antibody (pdb: 4I9W). (**A**) Schematic representation of 3.4 Å up state TREK-2 homodimer viewed in plane of membrane (*left*) and onto the cap from the extracellular side (*right*). (**B**) Stereo view of the electron density around the cap disulfide bridge. The 'omit' electron density map shown is calculated using the prime-and-switch method implemented in PHENIX (*46*) starting with a TREK-2 model that lacks the cap residues 118-127. The disulfide bridge between adjacent Cys[123] residues is highlighted in red. Two cadmium ions (Cd1/2) stabilize the cap domain via lattice contacts between EC1 helices of adjacent homodimers (**C**) Superposition of the domain-exchanged cap domains of TREK-2 (yellow/purple) and 2.75 Å TRAAK structure (4I9W, orange/dark cyan). (**D**) Schematic view of cap connectivity for domain-exchanged TREK-2 (orange/purple) and (**E**) non-exchanged TRAAK (pdb: 3UM7).
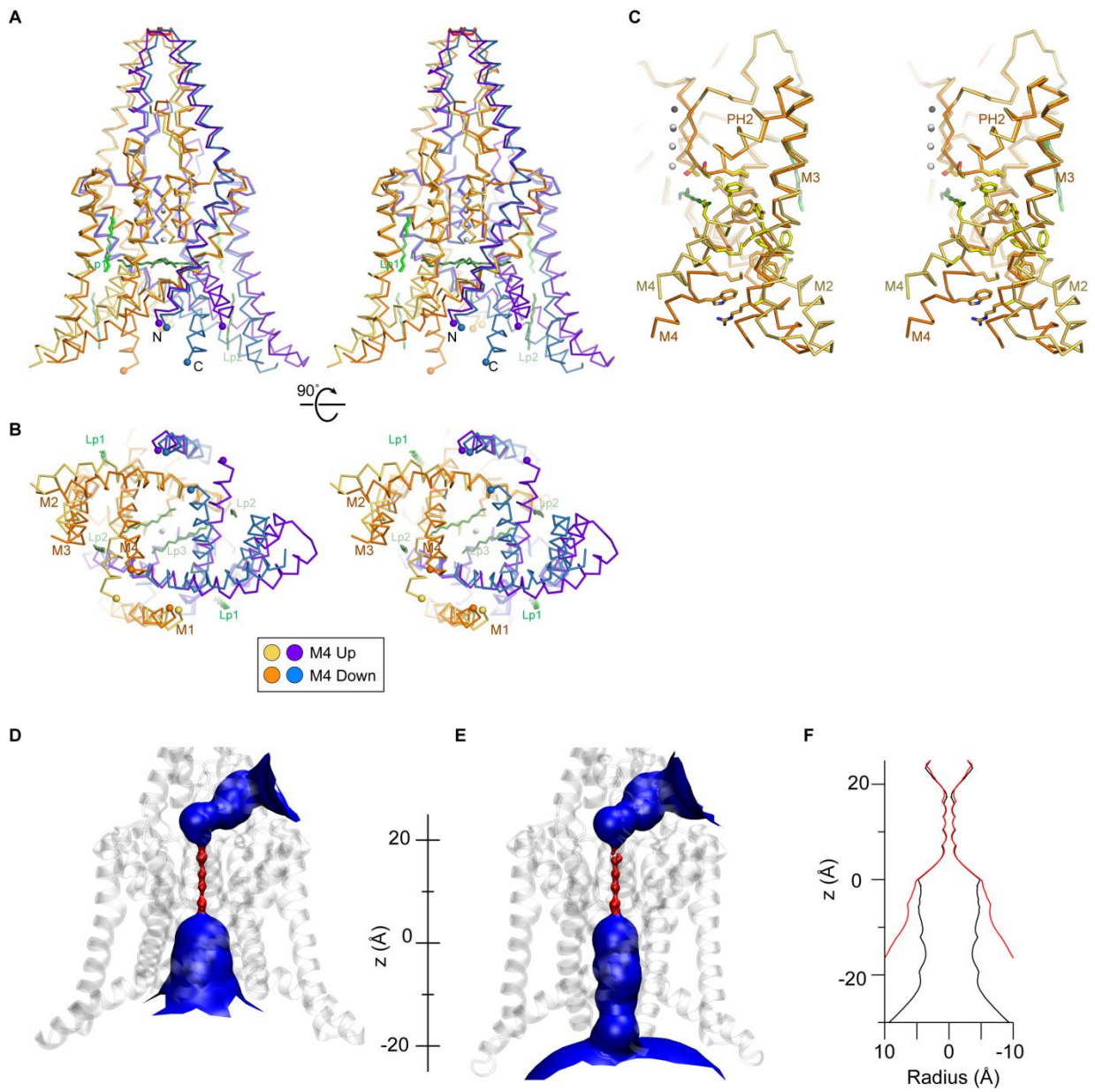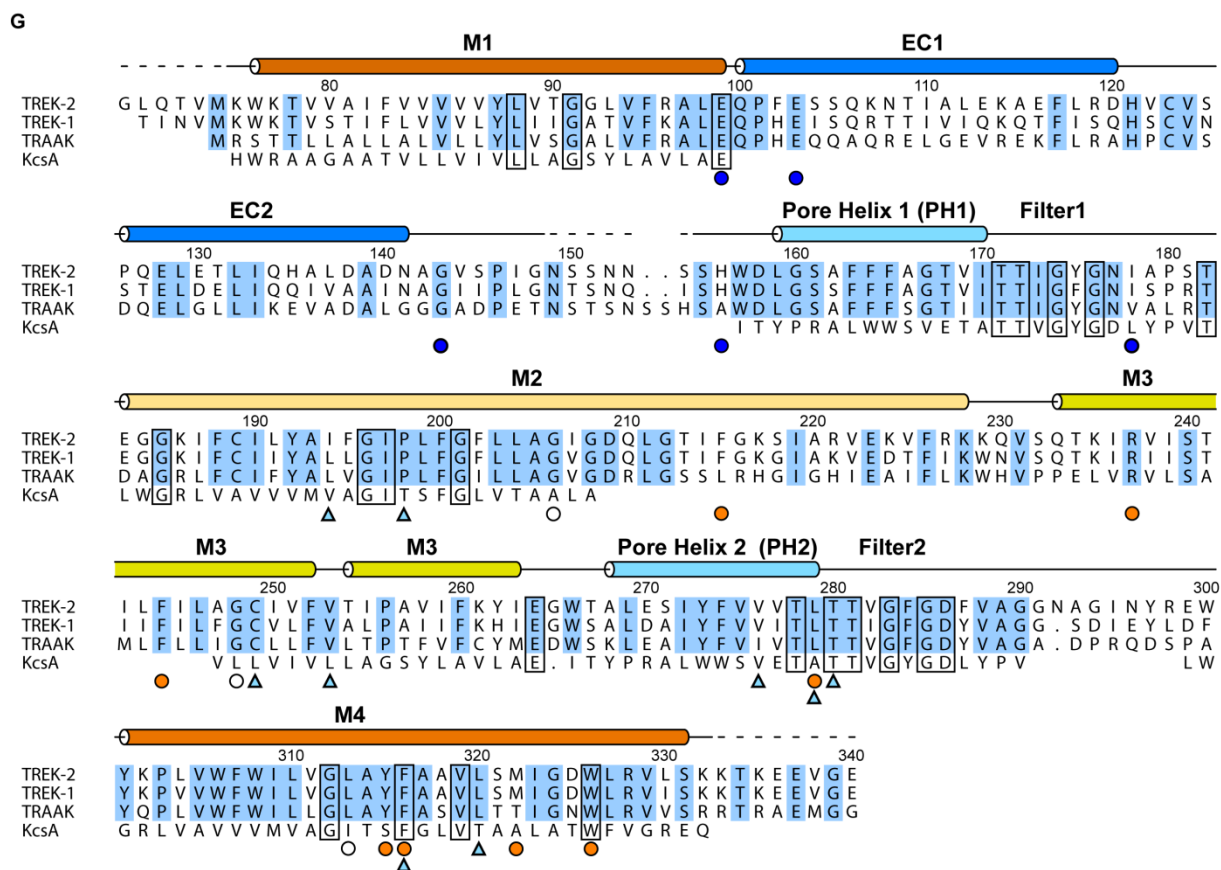
Fig. S5. Comparison of the up and down conformational states of TREK-2 and an alignment of the TREK, TRAAK and KcsA sequences. (**A**) Stereo view of TREK-2 channel homodimers viewed from the plane of the membrane. Modelled alkyl chains representing lipid fragments (Lp1-Lp3) are colored green. Fragment Lp1 is observed in both crystal forms whereas Lp2/3 are restricted to the 'down' conformation. (**B**) Stereo view looking from the intracellular face towards the pore. (**C**) Stereo view of superposed TREK-2 monomers for 'up' (yellow) and 'down' (orange) states. Hole (*56*) profiles displaying the radius of the pore in the up (**D**) and down state (**E**) of TREK-2. Blue represents regions of the ion path with a radius of >3.5 Å and red <1.2 Å. (**F**) Plot of the radius of the inner pore in the up (red) and down (black) states. (**G**) Sequence alignment of human tandem two pore K channels TREK-2, TREK-1 and TRAAK along with archetypal 2-TM KcsA. Only the M1/ Pore helix / filter / M2 regions of KcsA are shown based on structural superposition with TREK-2 model. Residues involved in the M2/3/4 hydrophobic clusters (orange circles), helix hinging residues (open circles), external pH sensor region (blue circles) and norfluoxetine binding site (cyan triangles) are highlighted.
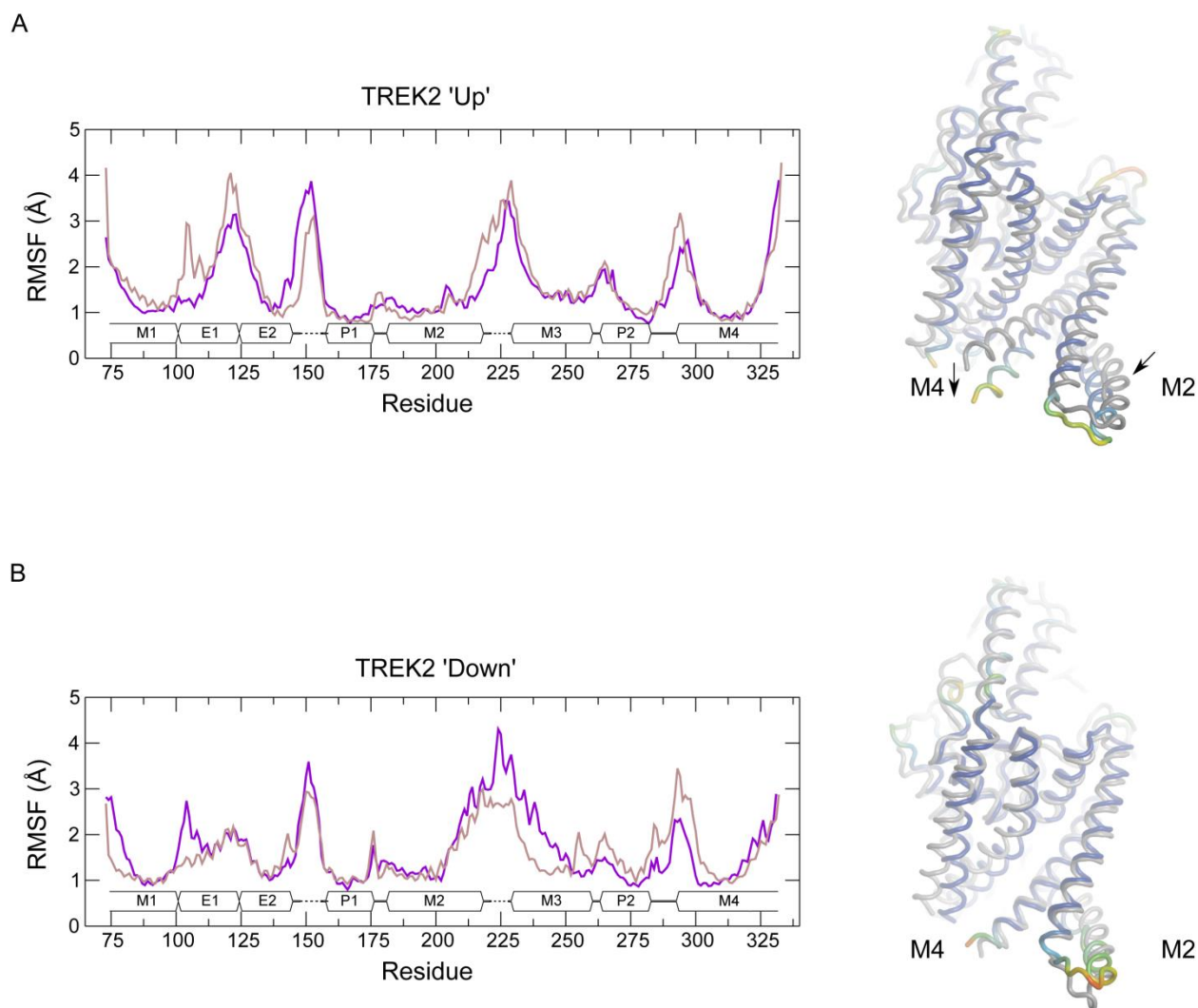
Fig. S6. Stability of 100ns MD simulation for TREK-2 up (A) and TREK-2 down (B) state structures in a lipid bilayer. Left panel: Averaged root mean square fluctuations (RMSF) calculated for backbone atoms of Chain A (purple) and Chain B (brown) from two 100 ns MD simulations versus residue number. The secondary structure of TREK-2 is also shown. Dashed lines represent regions missing in the crystal structures. Right panel: Tube representation of average structure from MD simulations colored by RMSF per residue (blue (small RMSF) through green to red (large RMSF)) superimposed on the starting structure (grey tube). Arrows indicate the movement of M4 and M2 in the up, but not down state simulations.
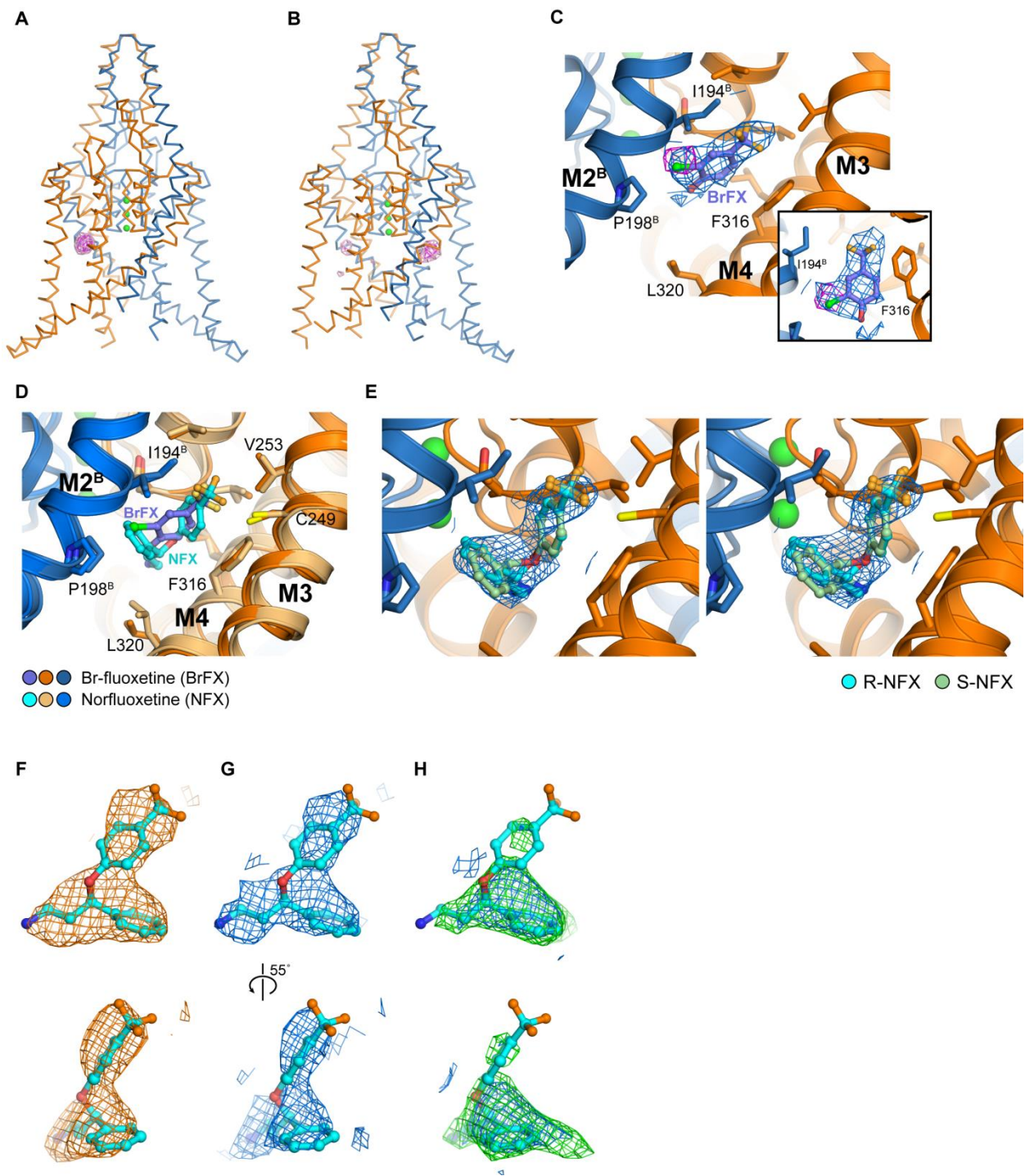
Fig. S7.

Fig. S7. Binding site for norfluoxetine unambiguously identified using anomalous signal from brominated derivative of fluoxetine. (A-B). Anomalous difference map calculated at 5Å for the Br-fluoxetine (Br-FX) dataset (collected at the Br K-edge) and shown with the C-α trace for each TREK-2 dimer within the asymmetric unit (chain A/C − orange; chain B/D − blue). The 5 Å anomalous difference map is contoured at 4.5σ (magenta) and 3σ (pink). A single anomalous peak, corresponding to the location of the bromine atom of Br-fluoxetine, is seen in the AB dimer while the CD dimer has two peaks. **(C)** Omit electron density for Br-fluoxetine. The RESOLVE density modified electron density (1σ, blue), calculated prior to ligand modelling, is shown with the 5 Å anomalous difference density (6.5σ, magenta). The brominated tri-fluoromethyl phenyl ring is well-defined in the electron density whereas the other two substituents are poorly resolved. **(D)** Comparison of the binding modes of Br-FX (lilac carbons) and norfluoxetine (NFX, cyan carbons). The binding site is viewed looking into the side fenestration between M4 and M2. Only the R-enantiomer of NFX is shown for clarity. **(E)** Stereo view showing the quality of the initial 3.7Å NFX electron density. The RESOLVE density modified electron density (blue; contoured at 1σ), calculated prior to ligand modelling, is shown for NFX along with the final model. As NFX used for crystallization is a racemic mixture, both R- and S-enantiomers were modelled. **(F-H)** Omit sigma-A weighted 2FoFc and FoFc electron density for the best defined NFX molecule (in the AB dimer). The electron density maps were calculated prior to inclusion of NFX in the refined model using RESOLVE **(F)**, REFMAC5 with map sharpening **(G)** and BUSTER **(H)**. Electron density maps are contoured at either 1σ (2FoFc) or 2σ (BUSTER FoFc map in (H); green).
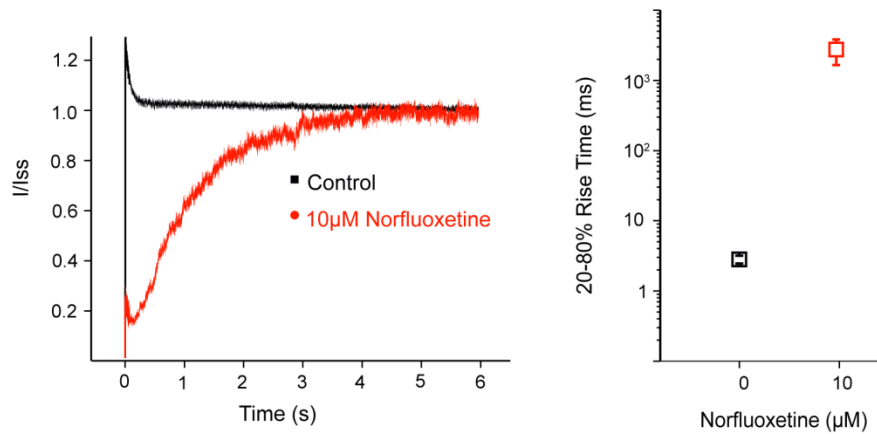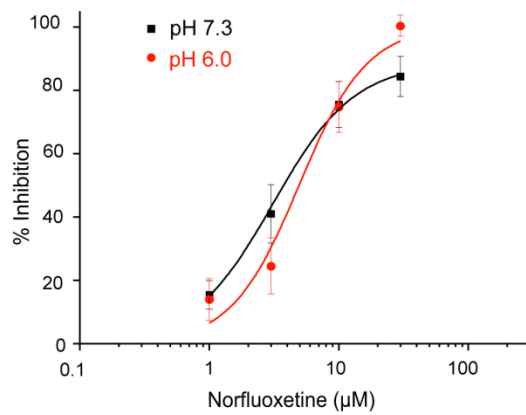
Fig. S8. Effect of norfluoxetine on the kinetics of TREK-2 activation by membrane stretch (-11 mmHg). (A) Left: In the absence of norfluoxetine rapid activation to a steady-state current occurs within a few milliseconds. However, in the presence of 10 μM norfluoxetine the activation of inhibitor-bound channels to a steady state current is dramatically slower. The time taken for activation from 20 % to 80 % of the maximum current is shown on the right and is 3 orders of magnitude slower in the presence of norfluoxetine. (**B**) By marked contrast to both stretch and AA activation (see Fig 2G), activation by pH_{int} (pH 6.0) does not alter norfluoxetine inhibition.
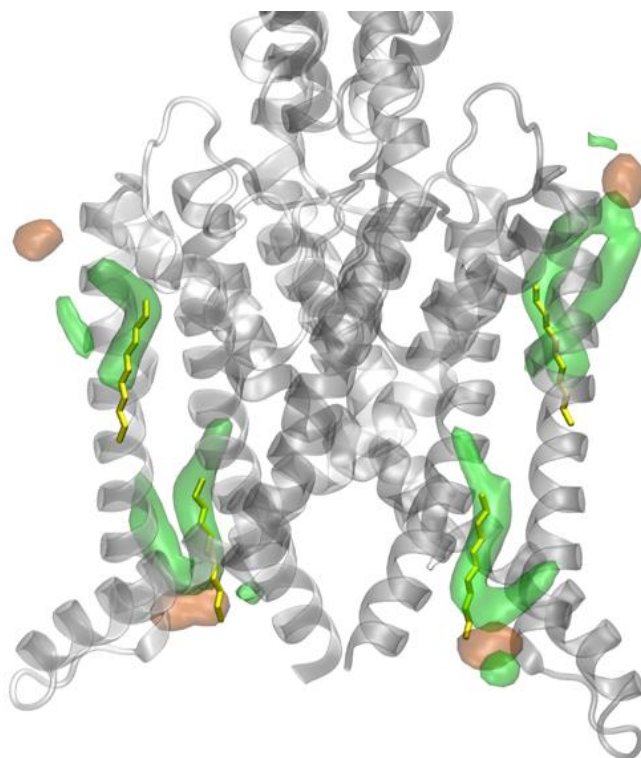
Fig. S9. MD simulations of lipid interactions. Lipid interaction during a 100 ns simulation with the protein positionally restrained. Transparent surface represents averaged density contour at 0.5 isosurface for carbon (green) and phosphorus (orange) atoms of lipids that interact at the sites overlaid onto the TREK-2 down state crystal structure. The modelled alkyl chains in the crystal structure are shown in stick representation (yellow). The high degree of overlap indicates that the alkyl chains modelled on the basis of elongated tubes of electron density probably represent immobilized lipids.

Fig. S10. Synthesis of Br-Fluoxetine.
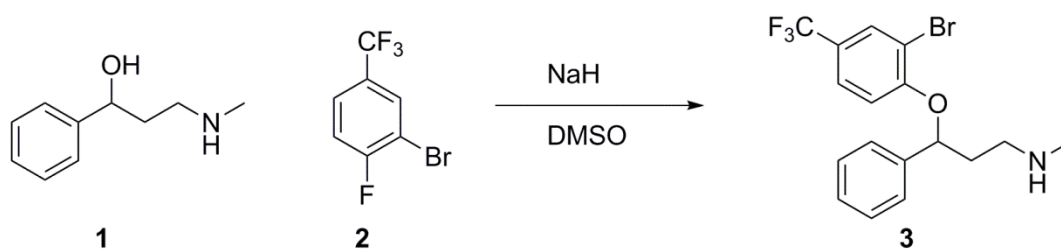
Movie S1. TREK-2 exhibits two distinct conformational states differing in the orientation of the transmembrane helices (M2-M4). The movie shows a linear transition between the up and down states of TREK-2, highlighting the structural differences between the two states and the concerted movement of the M2, M3 and M4 helices. A molecular surface representation illustrates the appearance of the lateral fenestrations observed in the down state structure. Norfluoxetine is shown in cpk representation binding in the fenestrations of the down state structure (cyan carbons). The models used for the movie have had missing loops that were not visible in the crystal structures reconstructed using structural information from other molecules in the asymmetric unit or from different crystal forms. The movie was created from a Cartesian morph between the up and down states calculated by UCSF-Chimera (*51*) and rendered using PyMol (*50*).

Table S1: Data collection, phasing and refinement statistics.

	Form 1/up state	Form 2/down state	Br-fluoxetine Complex	Norfluoxetine complex
PDB Code	4BW5			
Data Collection				
Space group	$P2_1$	$P2_1$	$P2_12_12_1$	$P2_1$
Cell dimensions				
a, b, c (Å)	87.83, 96.96, 103.7	76.75, 113.90, 111.80	101.71, 109.84, 166.74	75.19,113.03,112.50
α, β, γ (°)	90, 92.58, 90	90, 90.97, 90	90, 90, 90	90, 90.41, 90
Resolution [Å][1]	3.2 (3.20-3.28)[1]	3.8 (3.80-3.90)[1]	3.5 (3.50-3.59)[1]	3.6 (3.60-3.69)[1]
Resolution limits [Å][2]	4.10, 3.33, 3.20	4.05, 3.80, 3.97	3.55, 3.5 ,3.91	4.33, 3.6, 3.6
	(3.82, 3.20, 3.20)	(4.00, 3.80, 3.88)	(3.50,3.50,3.82)	(4.09, 3.6,3.6)
Nominal Resolution [Å][3]	3.4	3.9	3.64	3.7
$CC_{1/2}$	0.999 (0.436)	0.999 (0.579)	0.999 (0.553)	0.99 (0.685)
R_{meas}	0.062 (1.539)[1]	0.083 (0.971)[1]	0.097 (1.934)[1]	0.052 (0.931)[1]
$I / \sigma I$	10.7 (1.1)[1]	10.8 (1.8)[1]	17.5 (1.5)[1]	15.1 (1.8)[1]
Completeness [%]	99.4 (99.0)[1]	99.0 (99.5)[1]	99.9 (100)[1]	99.6 (99.6)[1]
Redundancy	3.8 (3.7)[1]	3.4 (3.4)[1]	11.4 (11.2)[1]	3.8 (4.0)[1]
Refinement				
Resolution (Å)	39.57 – 3.20	37.26 – 3.8	22.31-3.50	40.0-3.60
No. reflections (free)	28689 (1458)	18895 (978)	24074 (1215)	21816 (1127)
R_{work} / R_{free}	23.69 / 25.40	26.53 / 28.13	21.69/25.27	24.98/25.67
No. atoms				
Protein	7203	6895	7458	6821
Other	32	76	90	215
B-factors (Å^2)				
Protein	156	167	156	180
Other	133	118	166	206
Dimer AB	148	139	148	158
Dimer CD	163	194	164	205
R.m.s. deviations				
Bond lengths (Å)	0.009	0.009	0.009	0.009
Bond angles (°)	0.93	0.90	1.01	0.92

[1] Values in parentheses are statistics for highest resolution shell

[2] Anisotropic resolution limits along each of the three principal directions as defined by AIMLESS based on Mn (I/sd(I)) > 2. Values in parentheses are resolution limits in each direction based on half dataset correlation > 50% ($CC_{1/2}$).

[3] Nominal resolution is defined based on overall Mn (I/sd(I)) > 2 as estimated by AIMLESS.

Additional Author notes:

YYD and ACWP contributed equally to this project. YYD was responsible for purification optimization and preparation of protein, growth and optimization of crystals for the two unliganded conformations and for the norfluoxetine complex. ACWP supervised crystallization, mounted and screened crystals, collected diffraction data and solved and built the structures. AM was responsible for preparation of protein, growth and optimization of crystals for the Br-fluoxetine data and structure determination for this complex. CM was responsible for generation of the electrophysiology data. PA performed and MSPS and SJT supervised the MD simulations. AQ was responsible for running the HTP IMP pipeline and, together with MG and LD, generated initial expression and purification optimization data. SG cloned the constructs used in this experiment. SM produced large scale insect cell cultures and the baculovirus necessary for structure determination. GFR and PEB designed the synthesis of Br-fluoxetine, GFR synthesized and PEB supervised the synthesis of Br-fluoxetine. MVC and LC performed functional assays on purified TREK-2 using the Port-a-patch. CB initiated the project, helped in project management and helped prepare the manuscript. NABB was responsible for managing the pilot stages of this project, including cloning and test expression; and production of insect cells cultures. SJT was responsible for managing the electrophysiology and other functional data. EPC was responsible for managing all aspects of the structural work. She designed constructs, collected X-ray data and contributed to structure solution. YYD, ACWP, SJT and EPC analyzed the data and prepared the manuscript.

References and notes:

1.   P. Enyedi, G. Czirjak, Molecular background of leak K+ currents: two-pore domain potassium channels. *Physiol. Rev.* **90**, 559-605 (2010).

2.   A. Cohen, Y. Ben-Abu, N. Zilberberg, Gating the pore of potassium leak channels. *Eur. Biophys. J.* **39**, 61-73 (2009).

3.   A. Dedman *et al.*, The mechano-gated K(2P) channel TREK-1. *Eur. Biophys. J.* **38**, 293-303 (2009).

4.   J. Noel, G. Sandoz, F. Lesage, Molecular regulations governing TREK and TRAAK channel functions. *Channels (Austin)* **5**, 402-409 (2011).

5.   A. J. Patel, E. Honore, 2P domain K+ channels: novel pharmacological targets for volatile general anesthetics. *Adv. Exp. Med. Biol.* **536**, 9-23 (2003).

6.   A. Cadaveira-Mosquera, S. J. Ribeiro, A. Reboreda, M. Perez, J. A. Lamas, Activation of TREK currents by the neuroprotective agent riluzole in mouse sympathetic neurons. *J. Neurosci.* **31**, 1375-1385 (2011).

7.   C. Heurteaux *et al.*, Deletion of the background potassium channel TREK-1 results in a depression-resistant phenotype. *Nat. Neurosci.* **9**, 1134-1141 (2006).

8.   L. E. Kennard *et al.*, Inhibition of the human two-pore domain potassium channel, TREK-1, by fluoxetine and its metabolite norfluoxetine. *Br. J. Pharmacol.* **144**, 821-829 (2005).

9.   D. A. Bayliss, P. Q. Barrett, Emerging roles for two-pore-domain potassium channels and their potential therapeutic impact. *Trends Pharmacol. Sci.* **29**, 566-575 (2008).

10.   Z. Es-Salah-Lamoureux, D. F. Steele, D. Fedida, Research into the therapeutic roles of two-pore-domain potassium channels. *Trends Pharmacol. Sci.* **31**, 587-595 (2010).

11.   A. Mathie, E. L. Veale, Therapeutic potential of neuronal two-pore domain potassium-channel modulators. *Curr. Opin. Investig. Drugs* **8**, 555-562 (2007).

12.   M. E. Henry *et al.*, A comparison of brain and serum pharmacokinetics of R-fluoxetine and racemic fluoxetine: A 19-F MRS study. *Neuropsychopharmacology* **30**, 1576-1583 (2005).

13.   D. Thomas, B. Gut, G. Wendt-Nordahl, J. Kiehn, The antidepressant drug fluoxetine is an inhibitor of human ether-a-go-go-related gene (HERG) potassium channels. *J. Pharmacol. Exp. Ther.* **300**, 543-548 (2002).

14.   K. Furutani, Y. Ohno, A. Inanobe, H. Hibino, Y. Kurachi, Mutational and in silico analyses for antidepressant block of astroglial inward-rectifier Kir4.1 channel. *Mol. Pharmacol.* **75**, 1287-1295 (2009).

15.   I. Jeong, J. S. Choi, S. J. Hahn, Effects of fluoxetine on cloned Kv4.3 potassium channels. *Brain Res.* **1500**, 10-18 (2013).

16.   E. Honore, The neuronal background K2P channels: focus on TREK1. *Nat. Rev. Neurosci.* **8**, 251-261 (2007).

17.   A. Gurney, B. Manoury, Two-pore potassium channels in the cardiovascular system. *Eur. Biophys. J.* **38**, 305-318 (2009).

18.   M. Eckert, B. Egenberger, F. Doring, E. Wischmeyer, TREK-1 isoforms generated by alternative translation initiation display different susceptibility to the antidepressant fluoxetine. *Neuropharmacology* **61**, 918-923 (2011).

19. S. G. Brohawn, E. B. Campbell, R. MacKinnon, Domain-swapped chain connectivity and gated membrane access in a Fab-mediated crystal of the human TRAAK K+ channel. *Proc. Natl. Acad Sci. U. S. A*. **110**, 2129-2134 (2013).

20. S. G. Brohawn, J. del Marmol, R. MacKinnon, Crystal structure of the human K2P TRAAK, a lipid- and mechano-sensitive K+ ion channel. *Science* **335**, 436-441 (2012).

21. A. N. Miller, S. B. Long, Crystal structure of the human two-pore domain potassium channel K2P1. *Science* **335**, 432-436 (2012).

22. S. N. Bagriantsev, R. Peyronnet, K. A. Clark, E. Honore, D. L. Minor, Jr., Multiple modalities converge on a common gate to control K2P channel function. *EMBO J.* **30**, 3594-3606 (2011).

23. A. Mathie, E. Al Moubarak, E. L. Veale, Gating of two pore domain potassium channels. *J. Physiol.* **588**, 3149–3156 (2010).

24. P. L. Piechotta *et al.*, The pore structure and gating mechanism of K2P channels. *EMBO J.* **30**, 3607-3619 (2011).

25. M. Rapedius *et al.*, State-independent intracellular access of quaternary ammonium blockers to the pore of TREK-1. *Channels (Austin)* **6**, 473-478 (2012).

26. Materials and methods are available as supplementary materials on *Science* Online.

27. M. Zhou, J. H. Morais-Cabral, S. Mann, R. MacKinnon, Potassium channel receptor site for the inactivation gate and quaternary amine inhibitors. *Nature* **411**, 657-661 (2001).

28. E. Honore, F. Maingret, M. Lazdunski, A. J. Patel, An intracellular proton sensor commands lipid- and mechano-gating of the K(+) channel TREK-1. *EMBO J.* **21**, 2968-2976 (2002).

29. F. Maingret, A. J. Patel, F. Lesage, M. Lazdunski, E. Honore, Mechano- or acid stimulation, two interactive modes of activation of the TREK-1 potassium channel. *J. Biol. Chem.* **274**, 26691-26696 (1999).

30. S. N. Bagriantsev, K. A. Clark, D. L. Minor, Jr., Metabolic and thermal stimuli control K(2P)2.1 (TREK-1) through modular sensory and gating domains. *EMBO J.* **31**, 3297-3308 (2012).

31. J. Chemin *et al.*, Up- and down-regulation of the mechano-gated K(2P) channel TREK-1 by PIP (2) and other membrane phospholipids. *Pflugers Arch.* **455**, 97-103 (2007).

32. A. Anishkin, S. H. Loukin, J. Teng, C. Kung, Feeling the hidden mechanical forces in lipid bilayer is an original sense. *Proc. Natl. Acad. Sci. U. S. A.* **111**, 7898-7905 (2014).

33. S. G. Brohawn, Z. Su, R. MacKinnon, Mechanosensitivity is mediated directly by the lipid membrane in TRAAK and TREK1 K+ channels. *Proc. Natl. Acad. Sci. U. S. A.* **111**, 3614-3619 (2014).

34. J. Teng, S. Loukin, A. Anishkin, C. Kung, The force-from-lipid (FFL) principle of mechanosensitivity, at large and in elements. *Pflugers Arch.*, (2014).

35. G. Sandoz, D. Douguet, F. Chatelain, M. Lazdunski, F. Lesage, Extracellular acidification exerts opposite actions on TREK1 and TREK2 potassium channels via a single conserved histidine residue. *Proc. Natl. Acad. Sci. U. S. A.* **106**, 14628-14633 (2009).

36. Y. Kim, C. Gnatenco, H. Bang, D. Kim, Localization of TREK-2 K+ channel domains that regulate channel kinetics and sensitivity to pressure, fatty acids and pHi. *Pflugers Arch.* **442**, 952-960 (2001).

37. P. Aryal, F. Abd-Wahab, G. Bucci, M. S. Sansom, S. J. Tucker, A hydrophobic barrier deep within the inner pore of the TWIK-1 K2P potassium channel. *Nat. Commun.* **5**, 4377 (2014).

38. P. Aryal, M. S. Sansom, S. J. Tucker, Hydrophobic Gating in Ion Channels. *J. Mol. Biol.*, doi: 10.1016/j.jmb.2014.07.030. [Epub ahead of print] (2014).

39. S. Newstead, S. Ferrandon, S. Iwata, Rationalizing alpha-helical membrane protein crystallization. *Protein Sci.* **17**, 466-472 (2008).

40. J. L. Parker, S. Newstead, Current trends in alpha-helical membrane protein crystallization: an update. *Protein Sci.* **21**, 1358-1365 (2012).

41. T. M. Koenig, D. Mitchell, A convenient method for preparing enantiomerically pure norfluoxetine, fluoxetine and tomoxetine. *Tetrahedron Letters* **35**, 1339-1342 (1994).

42. W. Kabsch, Xds. *Acta Crystallogr. D Biol. Crystallogr.* **66**, 125-132 (2010).

43. P. Evans, Scaling and assessment of data quality. *Acta Crystallogr. D Biol. Crystallogr.* **62**, 72-82 (2006).

44. A. J. McCoy *et al.*, Phaser crystallographic software. *J. Appl. Crystallogr.* **40**, 658-674 (2007).

45. P. Emsley, B. Lohkamp, W. G. Scott, K. Cowtan, Features and development of Coot. *Acta Crystallogr. D Biol. Crystallogr.* **66**, 486-501 (2010).

46. P. D. Adams *et al.*, PHENIX: a comprehensive Python-based system for macromolecular structure solution. *Acta Crystallogr. D* **66**, 213-221 (2010).

47. G. Bricogne *et al.* (Global Phasing Ltd, Cambridge, UK, 2011).

48. V. B. Chen *et al.*, MolProbity: all-atom structure validation for macromolecular crystallography. *Acta Crystallogr D Biol Crystallogr* **66**, 12-21 (2010).

49. E. G. Hutchinson, J. M. Thornton, PROMOTIF--a program to identify and analyze structural motifs in proteins. *Protein Sci.* **5**, 212-220 (1996).

50. The PyMOL Molecular Graphics System, Version 1.5.0.4 Schrödinger, LLC.

51. E. F. Pettersen *et al.*, UCSF Chimera--a visualization system for exploratory research and analysis. *J. Comput. Chem.* **25**, 1605-1612 (2004).

52. A. Sali, T. L. Blundell, Comparative protein modelling by satisfaction of spatial restraints. *J. Mol. Biol.* **234**, 779-815 (1993).

53. P. J. Bond, J. D. Faraldo-Gomez, S. S. Deol, M. S. Sansom, Membrane protein dynamics and detergent interactions within a crystal: a simulation study of OmpA. *Proc. Natl. Acad. Sci. U. S. A.* **103**, 9518-9523 (2006).

54. C. Oostenbrink, A. Villa, A. E. Mark, W. F. van Gunsteren, A biomolecular force field based on the free enthalpy of hydration and solvation: the GROMOS force-field parameter sets 53A5 and 53A6. *J. Comput. Chem.* **25**, 1656-1676 (2004).

55. E. L. Veale *et al.*, Influence of the N terminus on the biophysical properties and pharmacology of TREK1 potassium channels. *Mol. Pharmacol.* **85**, 671-681 (2014).

56. O. S. Smart, J. G. Neduvelil, X. Wang, B. A. Wallace, M. S. Sansom, HOLE: a program for the analysis of the pore dimensions of ion channel structural models. *J. Mol. Graph.* **14**, 354-360, 376 (1996).